Simulating the dynamics of the mechanochemical cycle of myosin-V

Shayantani Mukherjee[a], Raphael Alhadeff[a], and Arieh Warshel[a,1]

[a]Department of Chemistry, University of Southern California, Los Angeles, CA 90089

Contributed by Arieh Warshel, January 6, 2017 (sent for review December 15, 2016; reviewed by Garegin A. Papoian and D. Thirumalai)

The detailed dynamics of the cycle of myosin-V are explored by simulation approaches, examining the nature of the energy-driven motion. Our study started with Langevin dynamics (LD) simulations on a very coarse landscape with a single rate-limiting barrier and reproduced the stall force and the hand-over-hand dynamics. We then considered a more realistic landscape and used time-dependent Monte Carlo (MC) simulations that allowed trajectories long enough to reproduce the force/velocity characteristic sigmoidal correlation, while also reproducing the hand-over-hand motion. Overall, our study indicated that the notion of a downhill lever-up to lever-down process (popularly known as the power-stroke mechanism) is the result of the energetics of the complete myosin-V cycle and is not the source of directional motion or force generation on its own. The present work further emphasizes the need to use well-defined energy landscapes in studying molecular motors in general and myosin in particular.

molecular motors | chemomechanical coupling | powerstroke | cytoskeleton | brownian ratchet

Myosin constitutes a superfamily of molecular motors comprising both the nonprocessive single-headed motors that are efficient in generating force on the actin filaments (e.g., myosin-II) and highly processive double-headed motors that can transport cellular load using tracks laid out by the cytoskeletal actin filaments (e.g., myosin-V, myosin-VI) (1, 2). The generation of force and unidirectional motion in each of the myosin molecules predominantly comprises tightly coupled events involving (*i*) binding and hydrolysis of ATP, followed by release of the products ADP and inorganic phosphate (P_i), occurring at the nucleotide-binding domain; (*ii*) binding and release of actin through the actin-binding domain; and (*iii*) a large conformational change of the lever arm that generates mechanical motion. Although the basic mechanochemical cycle is conserved in all members of the myosin superfamily, the exact nature of the coupling between the above steps in myosins, which decides the force-generating and load-bearing characteristics of different members, is unknown (*SI Background*).

Numerous experiments, including kinetics and thermodynamic studies (3), high-resolution structural studies (4), electron microscopy studies (5), atomic force microscopy (AFM), and single-molecule experiments (2, 6, 7), have advanced our understanding of the action of the system. Although details about the dynamical nature of the myosin-V, along with a quantitative knowledge of the force-response, have been learned from single-molecule studies, the structural studies have provided us with an atomistic knowledge of the key conformational states involved during the cycle, namely, the lever-up (pre) and lever-down (post) states (Fig. S1). In addition, crucial information has been gained on the kinetics of the chemical and ligand-binding/release steps that make up the complete cycle. Based on this experimental information, several theoretical modeling studies (8–17) explored the mechanochemical cycle, mostly using phenomenological modeling approaches, accompanied by some structure-based studies. One of the key ingredients used (almost always) in describing the unidirectionality and behavior under force in myosin-V is the nature of the conformational change, known as the powerstroke (PS), which is generally assumed to generate the force on actin filaments (18–20). The PS occurs in the leading leg (LL), where it changes conformation from the lever-up to lever-down position, although its ADP-bound head is still bound to the actin. On the other hand, the trailing leg (TL), which unbinds actin upon ATP binding, undergoes a conformational change from the lever-down to lever-up position, known as the recovery stroke (RS), and diffuses through the intermittent space between the previous and next actin-binding sites. It is frequently assumed that the PS must release the free energy that provides the basis for the directionality and resistivity of the motor against the force applied in the opposite direction. Unfortunately, the PS idea has not been demonstrated based on a clear, structure-based, free-energy landscape or by considering the principles of microscopic reversibility (21, 22). Apparently, it is extremely challenging to understand the free-energy balance of the myosin-V mechanochemical action. The challenge is due, in part, to the existence of several intermittent states in the cycle and the large size of the system, which make it inaccessible to atomistic simulations even with current computational power. In the absence of a complete understanding of the structure–function relationship of all of the steps in the whole functional cycle, the notion of a strain-dependent, free-energy–releasing PS has become a widely adopted conventional perspective in the field. Motor characteristics, such as directionality, stall force, force/velocity behavior, and other dynamical features of myosin, are usually described through this downhill lever arm movement. It is assumed implicitly that the free-energy release from ATP hydrolysis is transferred into structural strain in the legs (this strain develops especially after P_i release), which is then released through the lever arm movement of the PS (1). However, such a strained intermediate has not been established experimentally.

The PS is very difficult to observe experimentally as a separate process, uncoupled from the P_i release events. Most of the direct observations elucidate the strongly coupled nature of the P_i release and the lever arm movement (7, 23). Interestingly, although most experimental groups infer that the P_i must be released just before the PS (1), recent experiments also point to the possibility of the P_i being released after the PS (24). The authors have attempted to resolve these seemingly different observations and have suggested that the P_i might be trapped in another nonspecific protein site away from the catalytic center before it releases to the solvent (25).

Significance

The free-energy landscape of the complete mechanochemical cycle of myosin-V is used in simulating the real-time features of the directional motion. The combination of Langevin dynamics simulations and time-dependent Monte Carlo simulations reproduces the observed trend in terms of stall force and force/velocity profile. The present study also addresses the role of the powerstroke and finds it to be the result of the complete free-energy landscape rather than the driving force of the energy conversion by the system.

Author contributions: S.M., R.A., and A.W. designed research, performed research, analyzed data, and wrote the paper.

Reviewers: G.A.P., University of Maryland; and D.T., University of Texas at Austin.

The authors declare no conflict of interest.

[1]To whom correspondence should be addressed. Email: warshel@usc.edu.

This article contains supporting information online at www.pnas.org/lookup/suppl/doi:10.1073/pnas.1700318114/-/DCSupplemental.

This argument also highlights the point that the P_i-release free energy is tightly coupled to the PS and that we should understand the PS energetics in the context of the whole cycle. In our previous work (26), we have approached the problem by delineating the energetics of each of the steps that make up the whole cycle and then recombining the energetics and generating the free-energy surfaces for the forward and backward motion of the motor. This analysis has highlighted one interesting fact about the PS; namely, the conformation change from the lever-up to lever-down position is an energy-demanding process, whereas the RS occurring in the TL after ATP binding and actin release is an energy-releasing process. Despite a free energy demanding PS, the correct interweaving of the chemical free energies and actin-binding/release events with the PS and RS can generate several characteristics of myosin-V motion. To establish this finding in a more concrete way, it is important to explore the time dependence of the system. Thus, we studied here the dynamic behavior of the myosin-V model (proposed in ref. 26) under stochastic conditions, performing Langevin dynamics (LD) simulations of a 3D bead model of the motor on an effective free-energy surface and then performing Monte Carlo (MC) simulations of a model with explicit treatment of all chemical steps. Our results agree with the experimental observations of myosin-V and also produce the behavior under external force as indicated in numerous single-molecule studies. The crucial finding from this study is the fact that the PS does not have to be the energy-releasing step in order for myosin-V to function. Rather, in accordance with our previous study, the directionality and the stall force are decided by the relative overall barrier of the forward (plus-ended) over the backward (minus-ended) pathway. In short, our study supports the notion that myosin-V favors a Brownian-ratchet mechanism (21, 22) rather than a mechanical PS mechanism, which relies heavily on coupling the ATP hydrolysis free energy to mechanical strain-mediated conformational change (i.e., downhill PS).

Background

The Forward and Backward Cycle of Myosin-V. As in our previous study of myosin-V (26), we have delineated the energetics of the steps in the whole cycle using experimental kinetics data. The corresponding energetics were used to generate the free-energy landscape of the motor using a structure-based coarse-grained (CG) model (27, 28) that has been used to simulate various biological machines, such as F_OF_1-ATP synthase (29–31) and other systems (reviewed in ref. 27). The landscape combined the individual chemical and conformational steps in the correct order to produce motion toward the actin plus-end (forward) or minus-end (backward) direction, as shown in Fig. 1 for the forward motion and in Fig. S2 for the backward motion. In both figures, the starting state for the two pathways is the ADP-bound LL and nucleotide-free TL, both bound to actin. The figures involve a modification relative to the version reported by Mukherjee and Warshel (26) in terms of the height of the PS + P_i release barrier, because the observed rates could not discriminate between the two steps; that is, the combined barrier is less than 14.3 kcal/mol [larger than 200 s^{-1} in ref. (32)], although the results reported by Baker (33) suggested that the barrier for PS + P_i release is higher (additional discussion is provided in *Supporting Information*).

It is important to note that the forward and backward paths are not just microscopic reverses of each other; rather, the sequence of steps is different in the two pathways. The difference in the two paths stems from the asymmetrical energetics of performing the PS from the lever-up position, actin binding, and P_i release in the forward path [steps VI→(VIII) in Fig. 1] versus performing the ADP release, ATP binding, and PS from the lever-up position in the backward path [steps (VIII′)→(IX′)→(II′)→(III′)→(IV′) in Fig. S2]. The importance of different forward/backward paths in the workings of molecular motors in general has been discussed in depth (21, 22). In our model for myosin-V, the forward path is described by a chain of events starting with the TL binding ATP, releasing actin, performing the RS, and hydrolyzing the ATP, while diffusing in the plus-end direction. Meanwhile, the ADP-bound LL

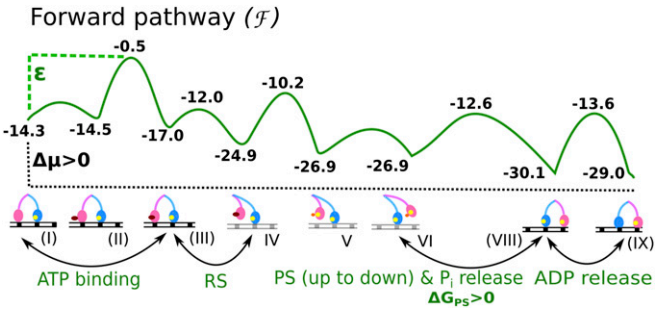

Fig. 1. Free-energy profile for a single step of myosin-V over actin filament along the forward positive-ended direction. The rate-limiting barrier along the path is indicated by ε.

remains strongly bound to actin and attempts to perform the energy-demanding PS conformational change. Until the TL releases its bound P_i and rebinds to its new actin position toward the plus end, the PS in the LL is not completely stabilized in this model. This result is in accordance with experimental observations that the PS in the LL is coupled to the P_i release and actin binding of the TL (7, 23). Once the TL is bound in its new actin position, it becomes the new LL with bound ADP, whereas the formerly called LL releases ADP and is poised to start a new cycle as the TL. The backward path, likewise, starts with the TL binding ATP, releasing actin, and hydrolyzing ATP, but performing the PS unsupported by the P_i release event (as opposed to the case in the forward path). This decoupling of the PS and P_i release can create a high-energy barrier (the red curve in Fig. S2) for the backward path, because the energy-demanding PS is not supported by any energy-releasing P_i release steps. On the contrary, the PS in the forward path is supported by the energy-releasing P_i step, and thus generates a much lower overall barrier along the path. We also note that the ADP release rate from the lever-down state (i.e., post-PS or rigor state) is slower than from the lever-up state (i.e., pre-PS state) (32, 34). The higher ADP release barrier along the backward path may also contribute to establishing directionality. The difference in the overall barrier ($\Delta\varepsilon = \varepsilon^* - \varepsilon$) occurring in the two pathways is sufficient to select the forward path over the backward path (26).

The movement of myosin-V can also be represented on an effective 2D free-energy landscape, as shown in Fig. 2 (details are provided in *Supporting Information*). Here, the horizontal direction corresponds to movement on the actin filament (plus- or minus-ended), whereas the vertical direction corresponds to the chemical events. The forward and backward paths depicted on the 2D surface also highlight the role of the barrier height (ε^* or ε) in determining the overall directionality of the motor. Although the nature of the directionality will be explored below, we also note that there is a current major interest in the reason for the dynamics and force behavior of myosin-V. Thus, we will also examine whether a downhill PS is essential for the dynamics, stall, and force/velocity characteristics of the motor, or if these characteristics emerge because of the complete free-energy landscape with proper mechanical and chemical coupling.

Modeling and Simulating Myosin-V. To explore the dynamics and directionality of myosin-V and its legs under the influence of the free-energy surfaces shown in Fig. 1 and Fig. S2, we used two complementary approaches. In the first approach, we have modeled the 3D system using multiple coarse-grained beads representing the motor legs joined with a common bead at the fork region. The double-legged myosin-V is then simulated using LD to walk over fixed actin-binding sites, separated by a fixed distance of 36 nm. In modeling this system, we had to consider the difficulties in long time simulations (even with CG models); thus, we used two complementary strategies. The first approach used a rather simple effective potential that groups together several contributions and allows one to explore the effect of the rate-limiting barriers in real 3D space

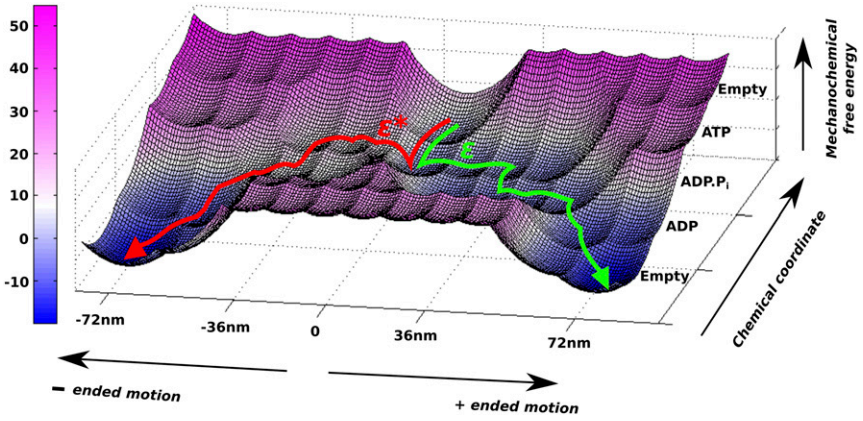

Fig. 2. Two-dimensional free-energy surface for the forward and backward motions. The green trajectory shows the most probable path taken by myosin-V during a single step over the energy barrier (ε) in the positive-ended direction, whereas the red trajectory is the corresponding backward motion toward the negative-ended direction over the high-energy barrier (ε*) landscape.

with general features resembling phenomenological descriptions but with much more connection to the complete surface. This model allowed us to explore the dynamics of the myosin system by LD simulations, albeit with scaled-down forward and backward barriers and much smaller diffusion coefficients. The details of the LD modeling are given in *Supporting Information*, Table S1, and Fig. S3.

In view of the difficulties of running the long time LD simulations needed to explore the force/velocity profile, we also introduce a second strategy based on a time-dependent MC approach with a more realistic free-energy surface. The landscape used is much closer to the landscape of Fig. 1 than the landscape used in the LD treatment. In brief, the MC simulations used a simplified myosin-V protein composed of three particles (two particles represent the two heads, and another joint particle represents their connection) moving along an actin filament. The use of only three particles is consistent with the important finding of Hinczewski et al. (12) that the arms behave as rigid rods. Additionally, we performed some calculations in a kinetic MC model, where the energy states (minima and maxima) from Fig. 1 were used to perform a 1D MC simulation, where the system can either move forward or backward along the energy landscape. The energies still had to be scaled down in both MC systems, but much less than in the LD simulations.

Results and Discussion

The Coupling of the P_i Release and the Lever Arm Movement of Myosin-V. One of our aims has been to explore whether having an energy-demanding PS interweaved with the chemical steps of ATP binding, P_i, and ADP release and actin-binding/release events can produce the myosin-V motion toward the plus end, as has been observed in numerous experiments (35–37). This issue was explored by running LD simulations under different conditions. The results of the simulations are described in Fig. 3, where Fig. 3*A* describes the motion of the motor center particle (joint) without any external load. Similar trajectories for the head particle starting as the TL and the head particle starting as the LL are shown in Fig. 3 *B* and *C*, respectively. It is observed that myosin-V walks in a hand-over-hand fashion with at least one leg bound to the actin filament. We also observe substep features (most evident in single-leg trajectories of Fig. 3 *B* and *C*), as found in single-molecule and AFM experiments (35, 36). The motion of the TL follows a substep of ∼40–50 nm, most of which is diffusive in nature after it releases the actin-binding site. The second substep of ∼20–30 nm occurs when the TL releases P_i and rebinds to the next actin-binding site. This rebinding moves the myosin head by one step in the plus-end direction. It is also observed that the completion of the energy-demanding PS occurring in the LL is almost always coupled with the P_i release and rebinding step of the TL, in close accordance with experimental findings (7, 23). Experiments have suggested that the PS can be reversed in the presence of high [P_i] in the bulk. This finding can be interpreted as inhibition of P_i release from the TL, leading to events of PS reversal rather than completion (23). We also note that a PS with large amount of free-energy release (as is often predicted to be the driving force in the PS mechanism) will occur in the LL as soon as the TL unbinds actin due to the presumed release of the mechanical constraint. In this case, inhibition of P_i release should not affect the fate of the PS in a severe way. On the contrary, an energy-demanding PS must be strongly coupled to the P_i release step to stabilize the lever-down state, as has been observed experimentally. It has been difficult to predict the exact sequence of events (P_i release and PS) in the motor during force generation. Most experimental groups favor P_i release before PS, citing structural considerations of difficulty in releasing P_i after the PS (1), although a recent group has reported P_i release after the PS step (24). As mentioned above, a recent review has also hypothesized that the released P_i can reside within the protein (in another distant nonspecific site) until the end of the PS; hence, P_i is released in the solution after the PS (25). Our results indicate that the energy-demanding PS is only stabilized (or ratcheted) with irreversible P_i release (irreversibility imposed under correct thermodynamic conditions of low ADP and P_i concentrations); hence, the PS could not be decoupled from the ligand-release kinetics. In other words, P_i release does not occur as a completely independent step before or after the PS; rather, it is more likely interleaved with the energy-demanding lever arm movement. The idea of intermediate P_i binding within the protein is an interesting concept (25), because it will allow the P_i free energy to release in steps, with a part being released soon after the electrostatic charge separation of the freshly cleaved gamma phosphate from the ADP alpha and beta phosphates and another part released after the P_i release into the solution (entropic in nature). This extended release of the P_i may allow

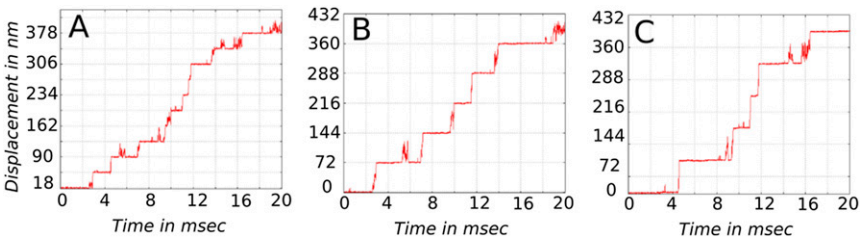

Fig. 3. Temporal dynamics of myosin-V in the unloaded condition are shown for the central bead (*A*), for the head particle of the leg starting as the TL (*B*), and for the head particle of the leg starting as the LL (*C*). Note that the central particle shows a displacement of 36 nm in a single step, whereas the head particles show displacement of 72 nm per step.

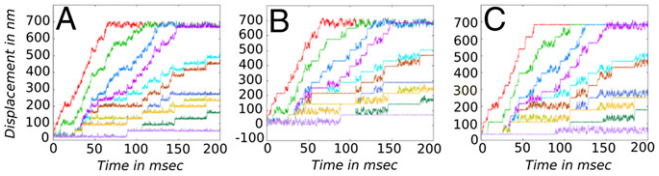

Fig. 4. Temporal dynamics of myosin-V in the loaded condition where force (F) is applied on the joint particle are shown for the central bead (*A*), for the head particle of the leg starting as the TL (*B*), and for the head particle of the leg starting as the LL (*C*). The color scheme of the trajectory plots with changing F are as follows: red (F = 0), green (F = 0.1 pN), blue (F = 0.2 pN), purple (F = 0.3 pN), cyan (F = 0.4 pN), brown (F = 0.5 pN), dark blue (F = 0.6 pN), olive (F = 0.7 pN), orange (F = 0.8 pN), dark green (F = 0.9 pN), and violet (F = 1.0 pN).

adequate coupling of the P_i release step to the high-energy–demanding PS during the forward motion.

Our simulations show that the TL rotates freely around the joint of the two legs during its diffusive motion before it rebinds to actin. This free rotation of the leg is also a result of the underlying angular constraint used on the joint. It was observed that a strong constraint on the joint led to nonproductive walking motion because the myosin-V was leaving the actin filament much earlier. The free rotation of the TL is in accordance with the motion observed in many single-molecule experiments on myosin-V (35, 36). Some of the trajectories have shown recursive motions of the TL, where the leg, instead of binding to the next actin-binding site, goes back to the previous site. This behavior of the TL has also been observed in the experiments and has been termed "foot stomping" (37). However, similar foot stomping of the LL is observed very rarely, where the LL sometimes rebinds to actin and initiates the walking motion, whereas it falls off and ceases the walking motion at other times. The rarity of LL foot stomping is mostly due to the leg being in a tight ADP- and actin-bound conformation compared with the TL, which releases ADP fast and binds a new ATP molecule to undergo actin release. The difference in ADP release rates in the LL and TL has been observed experimentally and suggested by some to be strain-mediated (32, 34). Overall, the trajectories reveal important mechanistic details about the hand-over-hand motion and substep features that match well-known experimental facts. Our results directly imply that myosin-V is capable of showing directional motion, not due to a free-energy–releasing conformational change (i.e., a downhill PS) but, instead, to proper coupling of the conformational free energies with the binding and product release steps. In this case, a high-energy–demanding PS in the LL is stabilized mostly by the P_i release in the TL, which also implies the strong connection between the PS and P_i release kinetics seen experimentally (23).

Dynamics of Myosin-V Under Constant Load: Dependence of Stall Force on the Pathway Barrier. One of our main goals is to reproduce the behavior of myosin-V under load. Accordingly, we carried out LD simulations under a constant load, varying from 0.1 to 1.0 pN, applied on the central particle (joint particle) in the opposite direction of the plus-end motion. Simulated trajectories for the loaded myosin are shown in Fig. 4 for the central particle and for the two head particles. It is observed that as the load increases, the number of steps taken by myosin-V reduces drastically with time, whereas the intermittent dwell times increase between consecutive steps. The nature of the mechanical motion (hand-over-hand motion and substep feature) is similar throughout the force regime explored in this study. All trajectories show a diffusive motion of the TL after it unbinds actin and rotates freely around the central particle before binding to the next site on the actin filament. Application of higher loads increases both the diffusive motion and the bound dwell time for the myosin-V legs. These results reveal that our model of myosin with an energy-demanding PS is actually capable of providing qualitatively similar walking motions as observed in experiments for both unloaded and loaded cases (35, 36). However, it should be noted that the time for a single myosin-V step is much faster in our simulations (especially the phase where both ADP-bound legs are bound to actin) compared with experimental observations. This observation is a result of very fast (almost instantaneous) ADP release and ATP binding in the TL (details are provided in *Supporting Information*), and has been done to speed up the simulations within reasonable computational resources.

Our next goal is to calculate the stall force from the unloaded and loaded simulations and to determine the dependence of the stall force on the parameters of the energy landscapes shown in Fig. 1 and Fig. S2. According to our model (26) and similar concepts explained elsewhere (21, 22), the most important parameter determining the directionality and stall force of chemically coupled molecular motors like myosin-V is the factor $\Delta\varepsilon = \varepsilon^* - \varepsilon$, namely, the difference in the barrier heights between the forward and backward pathways (further clarification of ε and ε^* is provided in Fig. 2).

We note once more, that the difference in the forward and backward barriers might arise from the asymmetry in the lever arm movement (energy-releasing up and energy-demanding down conformations) coupled to P_i release, as well as asymmetry in the ADP-release barriers in the up and down states. Whatever the exact origin of the higher barrier in the back motion, we explore the role of $\Delta\varepsilon$ under stochastic conditions by conducting forward and backward simulations using different values of $\Delta\varepsilon$. The stall force for each specific $\Delta\varepsilon$ value (obtained from forward simulation with ε and backward simulation with ε^*) is given by the force at which the ratio of backward (P_b) and forward (P_f) steps is 1 (i.e., $P_b/P_f = 1$). Fig. 5 *A* and *B* shows the exponential behavior of the P_b/P_f ratio for the force regime studied in this work and for different $\Delta\varepsilon$ values. It is seen that stall force increases with increasing $\Delta\varepsilon$. Due to the need for long time simulations to acquire sufficient statistics using a realistic 3D stochastic model, we have only calculated stall forces for $\Delta\varepsilon$ = 3, 4, 5, or 6 kcal/mol. The calculated stall forces are plotted in Fig. 5*C*, and the linear extrapolation yields a stall force of 2.3 pN for $\Delta\varepsilon = 8$ kcal/mol, whereas 11 kcal/mol (the value shown in Fig. 1) is on the higher end, giving a stall force of >3.5 pN. Because the experimental estimate on the stall force for myosin-V is in the range of 1–3 pN, we conclude that $\Delta\varepsilon$ should be in the range of 7–9 kcal/mol.

Higher Barrier MC Simulations. As stated in *Background*, in view of the difficulties of simulating long times, particularly in exploring the force/velocity profile, we introduced a time-dependent MC approach. The difficulties mentioned in *Background* are not so crucial while looking at the stall force that depends mainly on the overall rate-limiting barriers ε and ε^* and while investigating the dynamics of the legs during walking. However, the simulations of the force/velocity dependence may require a more detailed mechanochemical free-energy surface. Thus, in our MC approach, we use a more realistic free-energy surface, because we are not attempting to simulate the real-space 3D dynamics of the motor. The landscape used for the MC is presented in Figs. S4 and S5.

With the MC model, we can explore the nature of the observed force/velocity curve. Here, one can explore the possibility of interplay between different barriers to determine the rate. The

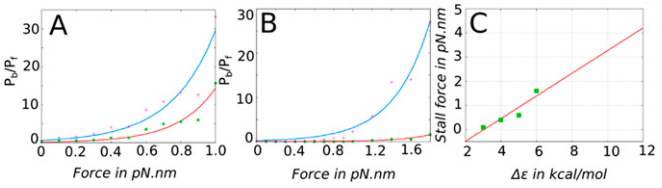

Fig. 5. P_b/P_f ratio (no. of forward steps/no. of backward steps calculated from trajectories of 200 ms) is plotted from trajectories of forward motion with force applied on the opposite direction (as in Fig. 4) and trajectories of backward motion with force applied on the same direction. Exponential fits for $\Delta\varepsilon = 3$ kcal/mol (blue) and 4 kcal/mol (red) (*A*) and for $\Delta\varepsilon = 5$ kcal/mol (blue) and 6 kcal/mole (red) (*B*) are shown. The stall force for each $\Delta\varepsilon$ is calculated as the force where $P_b/P_f = 1$. (*C*) Linear fit of these stall forces (plotted as green dots) for different $\Delta\varepsilon$ values.

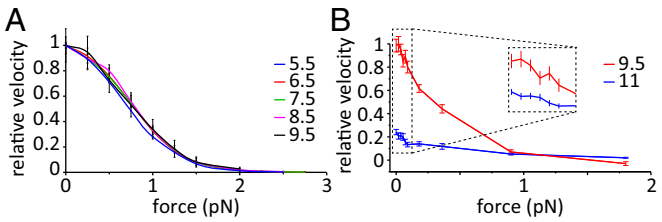

Fig. 6. (*A*) Force/velocity profile in the scaled 1D MC simulation as a function of the height of the highest barrier (ADP release). Scaling was done such that the ΔG values and the $\Delta\Delta g^{\ddagger}$ were maintained as much as possible (Fig. S6*B*). (*B*) Force/velocity profile in the 3D MC simulations. A zoom-in with vertical translation is provided for clarity.

most effective way to explore this issue is to use a 1D landscape in our MC model and to solve the kinetic problem. Doing so, we observed that it is not the absolute height of the barriers that defines the force/velocity profile but, rather, the difference between the highest barrier and the barrier where the force is applied ($\Delta\Delta g^{\ddagger}$). This fact is revealed by obtaining similar curves regardless of barrier scaling (Fig. 6*A*). To understand the criteria that dictate the shape of the force/velocity profile, we repeated this analysis using effective surfaces in which the height of the barrier where the force is applied is different, and it is apparent from Fig. S6*A* that a sigmoidal relationship requires a barrier that is relatively force-independent to be the rate-limiting barrier (e.g., the ADP release barrier compared with the PS + P_i release barrier).

Further, note that the effect of the force on the ADP release barrier may depend on the ADP concentration, because this concentration changes the relative height of the ADP release barrier and the PS + P_i release barrier (and this change can be reflected in the force effect). Interestingly, a broad plateau is achieved if $\Delta\Delta g^{\ddagger} >$ ~5 kcal/mol, whereas in our case, $\Delta\Delta g^{\ddagger} =$ ~3 kcal/mol.

Intuitively, the energy gap between the highest barrier (ADP release) and the barrier where the work is done to overcome the applied force (the PS + P_i release) is not large enough to make the latter barrier entirely negligible. Thus, the velocity is determined by a combination of both barriers. Initially, the highest barrier, which is relatively force-independent, is the dominant one, and the effect of the force is shielded by it; however, as the force increases, the dominant barrier becomes the PS + P_i release plus the work done to move against the force, and we encounter a decay in the velocity.

The use of the 3D CG model produced similar force/velocity profiles, where a sigmoid shape that is $\Delta\Delta g^{\ddagger}$-dependent can be seen (compare Fig. 6*B*, blue and red curves). The 3D MC trajectories are depicted in Fig. 7, with observed hand-over-hand and occasional foot-stomping dynamics.

Concluding Remarks

This work used a CG landscape of the myosin-V system and reproduced the directionality and other key observables by LD and MC simulations. These key observables include the stall force, the hand-over-hand dynamics, and the force/velocity profile. These findings add credibility to our view that the energetics of the lever arm movements (i.e., lever-up and lever-down conformational changes) in the RS and PS of the myosin are key ingredients for establishing the directionality, with another key ingredient being the asymmetry in ADP release rates in the different conformations.

Our study also allows us to explore the nature of the PS proposal; that is, although the PS proposal has not been formulated in a unique way in terms of the corresponding energy barriers and the way the force is generated, we may try to define and examine the main premises of this proposal. The central assumption of the PS proposition is that the strain developed in the actin-bound lever-up structure (assumed to occur after P_i release) is released during the lever-up to lever-down conformational change. This proposition leads to a free-energy–releasing PS that drives the load-dependent directional motion in myosin-V (1, 7, 16, 19, 38). However, our analysis shows that the energy of the lever-up to lever-down conformation is, in fact, increasing rather than decreasing [because the lever-up or pre-PS is the low-energy conformer, whereas the lever-down or post-PS is the high-energy conformer (26)].

We note that a significant part of the support in the PS model seems to come from the implicit assumption that the free-energy difference of the lever movement determines the directionality and efficiency, ignoring several aspects such as the intermediate barriers, coupling to chemical steps and imposing microscopic reversibility on correctly coupled mechanochemical events (21, 22). It also seems to us that some researchers assume that the forward lever arm movement involves an inertial motion [e.g., the statement that "rapid changes are essential" (39)], where the kinetic energy drives the directionality and generates force against a load. This assumption has some similarity to the assumption that dynamics drive enzyme catalysis by having an inertial model in which the kinetic energy of the binding process is used to drive the motion in the chemical direction (40). However, in the case of enzyme dynamics, it is simple to show that the kinetic energy fully dissipates before we have the chance for a stochastic fluctuation that climbs over the chemical activation free energy. It may be harder to see why the situation should be different in the case of the PS. The PS and related ideas imply a release of strain that is generally associated with van der Waals interactions. However, in biological systems, it is much more likely that the energy changes will be associated with slowly varying electrostatic energy, especially for those energy changes that involve long-range movements where the kinetic energy arising due to any van der Waals steric clashes are dissipated very quickly.

Another problematic assumption is the idea (e.g., ref. 20) that the effect of the PS is defined as the ratio between the input energy from ATP hydrolysis and the resulting work; that is, as shown in our study of the torque generation in ATPase (31), the relation of the work to the chemical energy is determined by the shape of the landscape in the conformational and chemical space. Of course, there are many dimensions, except the axis of the actin, where the chemical energy can be dissipated without doing any work along the PS coordinate (e.g., opening of the ATP site is perpendicular to this motion). In fact, recent work of Muretta et al. (24) agrees that the most important energetics are associated with P_i release and not with the large structural reorientation of the light-chain domain. Similarly, our finding supports the idea (21, 22) that the downhill strain-releasing PS motion is not the origin of the directionality or the basis of other motor characteristics.

The present work found that the observed force/velocity profile can be reproduced with the profile of Fig. 1. Notably, the sigmoidal profile is reproduced only when the PS + P_i release is not rate-limiting under low force. This finding further establishes the key role of the landscape in controlling the efficiency and force-dependent action of myosin motors. Considering the role of myosins, and specifically myosin-V, a landscape that is not too heavily dependent on the force is beneficial. In biological terms, when myosin-V is pulling different loads, it might experience a fairly large range of

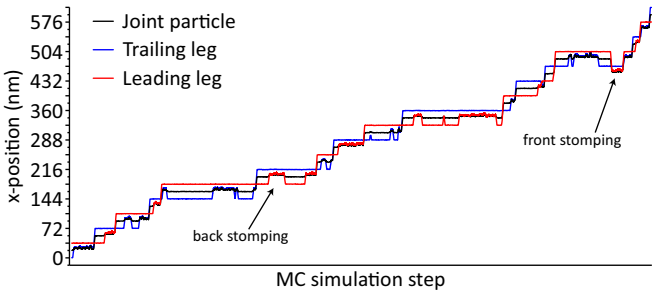

Fig. 7. Temporal dynamics in the 3D MC, presenting the *x* position of the myosin particles. Typically, a rough line indicates an unbound myosin head particle. Note that the TL and LL are colored based on the initial position and alternate roles on each step.

forces at time, and from a regulation point of view, having stable velocity, which probably affects the processibility as well, is better.

Our LD simulations indicated that the difference between the backward and forward barriers can be smaller than predicted in our previous work (26), although still allowing for the observed hand-over-hand dynamics, substep features, stall force, and dynamical behavior under force. To explore this issue more fully, we need to have more details about the landscape for the backward motion. In this respect, we note an interesting point that has not been resolved fully in the present work, that is, the nature of the barrier in the backward motion. As indicated in Fig. S2, the height of the backward barrier can depend on the point where the lever arm changes from a lever-up to lever-down conformation, leading to an increase in energy. If the lever-up to lever-down conformation occurs late and in concert with the P_i release, we may obtain the blue line in Fig. S2. In this case, it is likely that the combined PS + P_i release barrier of the backward-walking leg will not be so high, and it is also possible that the backward motion is controlled by the asymmetry in the ADP release barriers in the lever-up and lever-down states. On this subject, it is interesting to note that although ADP release rates have been proposed to be strain-dependent (32, 34), we hypothesize that the difference in ADP release rates for the prestate and poststate is a result of the conformational changes imposed in and around the binding sites of TL or LL, and might not be directly coupled to the applied force. Rather, the applied force in the opposite direction on the LL can act to populate the prestate more than the poststate, and thus might affect the ADP release rates differently in the LL compared with the TL. In any case, exploring the actual origin of the backward barrier would require more careful and explicit simulation studies involving structural considerations of the motor. It will also be exciting to find experimental ways to explore this issue. Whatever may be the origin of the high back barrier, our study highlights that a relative barrier difference (between forward and backward paths) can produce the observed directional motion and the stall force. Additionally, the high-energy–releasing PS is completely consistent with the myosin dynamics and its coupling to the P_i release step further allows control of its force-dependent characteristics by altering the ligand release kinetics in different subfamilies of myosin. Overall, we believe that the present work should further emphasize the crucial need of having a clear idea of the complete mechanochemical free-energy landscape when exploring the action of molecular machines.

Methods

This work uses the CG landscape of the study by Mukherjee and Warshel (26) and explores the corresponding dynamics by LD simulations that are described in the main text and *Supporting Information*. The nature of the long time behavior of the system was explored by an MC approach that is also described in the main text, *Supporting Information*, and Figs. S6*B* and S7.

ACKNOWLEDGMENTS. We thank Dr. Dean Astumnian for instructive discussions. We thank the University of Southern California High Performance Computing and Communication Center for computational resources. This work was supported by National Science Foundation Grant MCB-0342276.

1. Sweeney HL, Houdusse A (2010) Structural and functional insights into the Myosin motor mechanism. *Annu Rev Biophys* 39:539–557.
2. Mehta AD, et al. (1999) Myosin-V is a processive actin-based motor. *Nature* 400(6744): 590–593.
3. De La Cruz EM, Ostap EM (2004) Relating biochemistry and function in the myosin superfamily. *Curr Opin Cell Biol* 16(1):61–67.
4. Coureux PD, Sweeney HL, Houdusse A (2004) Three myosin V structures delineate essential features of chemo-mechanical transduction. *EMBO J* 23(23):4527–4537.
5. Wulf SF, et al. (2016) Force-producing ADP state of myosin bound to actin. *Proc Natl Acad Sci USA* 113(13):E1844–E1852.
6. Yildiz A, et al. (2003) Myosin V walks hand-over-hand: Single fluorophore imaging with 1.5-nm localization. *Science* 300(5628):2061–2065.
7. Sellers JR, Veigel C (2010) Direct observation of the myosin-Va power stroke and its reversal. *Nat Struct Mol Biol* 17(5):590–595.
8. Lan G, Sun SX (2005) Dynamics of myosin-V processivity. *Biophys J* 88(2):999–1008.
9. Yu H, Ma L, Yang Y, Cui Q (2007) Mechanochemical coupling in the myosin motor domain. II. Analysis of critical residues. *PLOS Comput Biol* 3(2):e23.
10. Navizet I, Lavery R, Jernigan RL (2004) Myosin flexibility: Structural domains and collective vibrations. *Proteins* 54(3):384–393.
11. Craig EM, Linke H (2009) Mechanochemical model for myosin V. *Proc Natl Acad Sci USA* 106(43):18261–18266.
12. Hinczewski M, Tehver R, Thirumalai D (2013) Design principles governing the motility of myosin V. *Proc Natl Acad Sci USA* 110(43):E4059–E4068.
13. Zheng W (2011) Coarse-grained modeling of conformational transitions underlying the processive stepping of myosin V dimer along filamentous actin. *Proteins* 79(7): 2291–2305.
14. Kolomeisky AB, Fisher ME (2007) Molecular motors: A theorist's perspective. *Annu Rev Phys Chem* 58:675–695.
15. Bierbaum V, Lipowsky R (2011) Chemomechanical coupling and motor cycles of myosin V. *Biophys J* 100(7):1747–1755.
16. Vilfan A (2005) Elastic lever-arm model for myosin V. *Biophys J* 88(6):3792–3805.
17. Tehver R, Thirumalai D (2010) Rigor to post-rigor transition in myosin V: Link between the dynamics and the supporting architecture. *Structure* 18(4):471–481.
18. Wang H, Oster G (2002) Ratchets, power strokes, and molecular motors. *Appl Phys A Mater Sci Process* 75(2):315–323.
19. Howard J (2001) *Mechanics of Motor Proteins and the Cytoskeleton* (Sinauer, Sunderland, MA), pp 76–89.
20. Wagoner JA, Dill KA (2016) Molecular motors: Power strokes outperform Brownian ratchets. *J Phys Chem B* 120(26):6327–6336.
21. Astumian RD, Mukherjee S, Warshel A (2016) The physics and physical chemistry of molecular motors. *ChemPhysChem* 17(12):1719–1741.
22. Astumian RD (2015) Irrelevance of the power stroke for the directionality, stopping force, and optimal efficiency of chemically driven molecular machines. *Biophys J* 108(2):291–303.
23. Kad NM, Trybus KM, Warshaw DM (2008) Load and Pi control flux through the branched kinetic cycle of myosin V. *J Biol Chem* 283(25):17477–17484.
24. Muretta JM, Rohde JA, Johnsrud DO, Cornea S, Thomas DD (2015) Direct real-time detection of the structural and biochemical events in the myosin power stroke. *Proc Natl Acad Sci USA* 112(46):14272–14277.
25. Houdusse A, Sweeney HL (2016) How myosin generates force on actin filaments. *Trends Biochem Sci* 41(12):989–997.
26. Mukherjee S, Warshel A (2013) Electrostatic origin of the unidirectionality of walking myosin V motors. *Proc Natl Acad Sci USA* 110(43):17326–17331.
27. Vicatos S, Rychkova A, Mukherjee S, Warshel A (2014) An effective coarse-grained model for biological simulations: Recent refinements and validations. *Proteins* 82(7): 1168–1185.
28. Messer BM, et al. (2010) Multiscale simulations of protein landscapes: Using coarse-grained models as reference potentials to full explicit models. *Proteins* 78(5): 1212–1227.
29. Mukherjee S, Warshel A (2011) Electrostatic origin of the mechanochemical rotary mechanism and the catalytic dwell of F1-ATPase. *Proc Natl Acad Sci USA* 108(51): 20550–20555.
30. Mukherjee S, Warshel A (2012) Realistic simulations of the coupling between the protomotive force and the mechanical rotation of the F0-ATPase. *Proc Natl Acad Sci USA* 109(37):14876–14881.
31. Mukherjee S, Bora RP, Warshel A (2015) Torque, chemistry and efficiency in molecular motors: A study of the rotary-chemical coupling in F1-ATPase. *Q Rev Biophys* 48(4): 395–403.
32. Rosenfeld SS, Sweeney HL (2004) A model of myosin V processivity. *J Biol Chem* 279(38):40100–40111.
33. Baker JE, et al. (2004) Myosin V processivity: Multiple kinetic pathways for head-to-head coordination. *Proc Natl Acad Sci USA* 101(15):5542–5546.
34. Veigel C, Schmitz S, Wang F, Sellers JR (2005) Load-dependent kinetics of myosin-V can explain its high processivity. *Nat Cell Biol* 7(9):861–869.
35. Dunn AR, Spudich JA (2007) Dynamics of the unbound head during myosin V processive translocation. *Nat Struct Mol Biol* 14(3):246–248.
36. Andrecka J, et al. (2015) Structural dynamics of myosin 5 during processive motion revealed by interferometric scattering microscopy. *eLife* 4:4.
37. Kodera N, Yamamoto D, Ishikawa R, Ando T (2010) Video imaging of walking myosin V by high-speed atomic force microscopy. *Nature* 468(7320):72–76.
38. Tyska MJ, Warshaw DM (2002) The myosin power stroke. *Cell Motil Cytoskeleton* 51(1):1–15.
39. Houdusse A, Sweeney HL (2001) Myosin motors: Missing structures and hidden springs. *Curr Opin Struct Biol* 11(2):182–194.
40. Kamerlin SCL, Warshel A (2010) At the dawn of the 21st century: Is dynamics the missing link for understanding enzyme catalysis? *Proteins* 78(6):1339–1375.
41. Pisliakov AV, Cao J, Kamerlin SCL, Warshel A (2009) Enzyme millisecond conformational dynamics do not catalyze the chemical step. *Proc Natl Acad Sci USA* 106(41): 17359–17364.
42. Liu H, Shi Y, Chen XS, Warshel A (2009) Simulating the electrostatic guidance of the vectorial translocations in hexameric helicases and translocases. *Proc Natl Acad Sci USA* 106(18):7449–7454.
43. Metropolis N, Rosenbluth AW, Rosenbluth MN, Teller AH, Teller E (1953) Equation of state calculations by fast computing machines. *J Chem Phys* 21(6):1087–1092.
44. Kamerlin SCL, Warshel A (2010) The EVB as a quantitative tool for formulating simulations and analyzing biological and chemical reactions. *Faraday Discuss* 145:71–106.